A second generation of low thermal noise cryogenic silicon resonators

D G Matei[1,3], T Legero[1], Ch Grebing[1], S Häfner[1], Ch Lisdat[1], R Weyrich[1], W Zhang[2], L Sonderhouse[2], J M Robinson[2], F Riehle[1], J Ye[2] and U Sterr[1]

[1]Physikalisch-Technische Bundesanstalt (PTB), Bundesallee 100, 38116 Braunschweig, Germany
[2]JILA, National Institute of Standards and Technology and University of Colorado, 440 UCB, Boulder, CO 80309-0440, USA

[3]Corresponding author: dan.matei@ptb.de

Abstract. We have set up an improved vertically mounted silicon cavity operating at the zero-crossing temperature of the coefficient of thermal expansion (CTE) near 123 K with estimated thermal noise limited instability of 4×10^{-17} in the modified Allan deviation. Owing to the anisotropic elasticity of single-crystal silicon, the vertical acceleration sensitivity was minimized *in situ* by axially rotating the resonator with respect to the mounting frame. The control of the resonator temperature is greatly improved by using a combination of two thermal shields, monitoring with several temperature sensors, and employing low-thermal conductivity materials. The instability of the resonator stabilized laser was characterized by comparing with another low-noise system based on a 48 cm long room temperature cavity of PTB's strontium lattice clock, resulting in a modified Allan deviation of 7×10^{-17} at 100 s.

1. Introduction

Even today's most stable lasers only achieve a coherence time of a few seconds, which are still at least an order of magnitude away from the coherence time of the clock transitions in neutral atoms or ions that are employed in the best optical clocks [1,2]. Thus, at present, the resolved linewidths of these clock transitions are mostly limited by the frequency fluctuations of the interrogating laser. In addition, in a discontinuous interrogation of the clock transition, frequency fluctuations further decrease the clock stability via the Dick effect [3].

While promising results have been obtained from alternative laser stabilization methods like spectral hole burning [4] or active clocks [5], the longest coherence times are provided by laser systems stabilized to optical cavities. Thermal noise fundamentally limits the length stability of optical cavities and thus the frequency stability of ultrastable lasers that use cavities as a frequency reference [6]. To reduce the influence of thermal noise, various approaches have been followed, such as increasing the cavity length [7], lowering the temperature [8,9], or using spacer and coating materials with high mechanical quality factor [10].

Extending previous work based on PTB-JILA collaboration [8,11], we are setting up two nearly identical silicon cavities that operate at the zero-crossing temperature of the thermal expansion coefficient (CTE) near 123 K [12] with estimated thermal noise limited instability of mod $\sigma_y \approx 4\times10^{-17}$. Here we report on the first of the two improved cryogenic silicon resonators. For comparison, we employ another ultra-low thermal noise system at 698 nm, based on a 48 cm long ULE spacer with dielectric

mirror coatings on fused silica substrates. The comparison includes a frequency comb and noise cancelled fiber links between the systems. In previous three-cornered-hat comparisons, the ULE system achieved an instability of $\sigma_y = 8\times10^{-17}$ [7].

Throughout this paper we use the modified Allan deviation for analysis, since the comparison between the 1.5 μm laser and the 698 nm laser is affected by high-frequency phase noise from the frequency comb [13] and from the limited servo bandwidth of the frequency lock to the cavity. In this case the standard Allan deviation depends on the measurement bandwidth while the modified Allan deviation does not show this ambiguity. In addition, its steeper slope clearly allows identifying low-frequency fluctuations [14].

2. Cavity setup and reduction of technical noise

The most important technical noise sources which degrade the laser performance are seismic and acoustic vibrations, pressure and temperature fluctuations and residual amplitude modulation (RAM). To reduce these influences we re-engineered the first generation silicon resonator system [8]. As a first step we significantly increased the cavity finesse of the TEM_{00} mode to 480 000 by replacing the contaminated mirrors. This provides better tolerance against RAM and electronic offsets in the Pound-Drever-Hall (PDH) [15] servo setup. The additional improvements to the cavity support structure, the vacuum, and the temperature control are presented in detail in the following.

2.1. Silicon cavity mounting

As in the previous setup [8], a double-cone shaped single-crystal silicon cavity with a length of 21 cm is used with its vertical optical axis parallel to the <111> direction of the silicon crystal. The cavity is placed on an optimized tripod mount as shown in figure 1a. A support ring made of silicon decouples the cavity from the thermal expansion of the base plate. The ring is connected by three polyether ether ketone (PEEK) rods to the base plate and supports the spacer on three small PEEK posts.

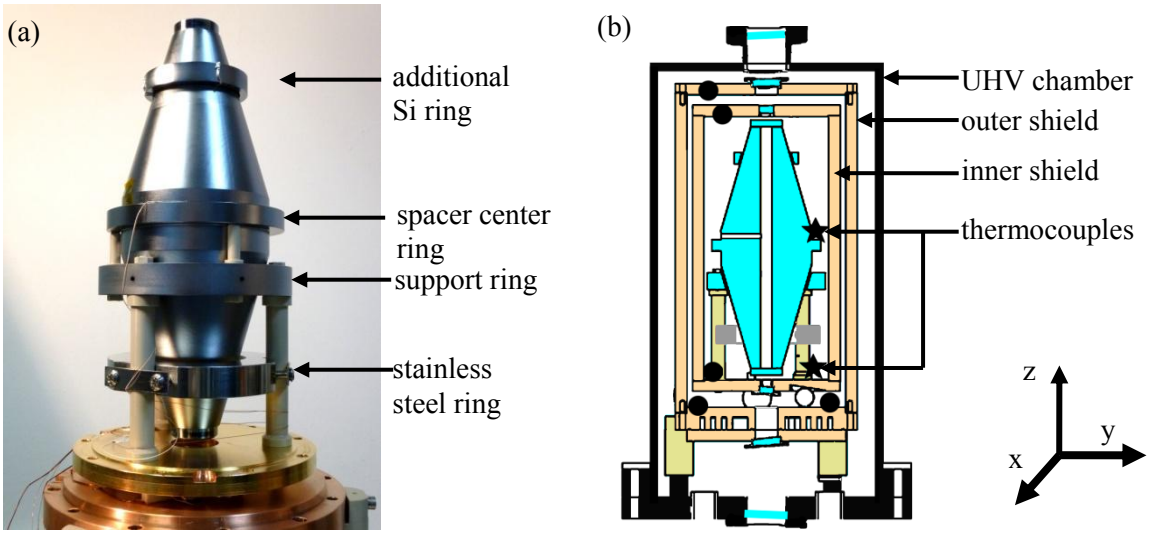

Figure 1. (a) Silicon spacer with the optimized tripod support frame on the two bottom plates of the heat shields. (b) Cross section of the cryostat, showing the cavity inside the two heat shields. The positions of the temperature sensors are indicated with arrows: Pt100 resistors (full circles) and the thermocouple junction on the spacer (star); (Colour online).

Any mechanical resonances in the support structure enhance vibrations acting on the cavity. As a result of replacing the polytetrafluoroethylene (PTFE) support structure used in [8] with PEEK and adding a stainless steel clamping ring, the lowest FEM-simulated mechanical resonance frequency is now moved from 15 Hz to above 70 Hz at room temperature, away from the noisy region in the vibration spectrum (figure 2b).

The vibration sensitivity was measured by applying sinusoidal accelerations along the x, y or z direction and observing the corresponding optical frequency change with respect to a stable reference laser. With the improved support frame we found at 5 Hz excitation frequency horizontal sensitivities of $k_x = 2.5(12)\times10^{-12}$ $(m/s^2)^{-1}$ and $k_y = 0.7(6)\times10^{-12}$ $(m/s^2)^{-1}$. The residual sensitivity to horizontal accelerations can be attributed to related bending of the spacer in combination with an offset of the cavity mode from the symmetry axis [16]. Also asymmetries in the elastic properties of the tripod lead to radial forces on the spacer that will affect the cavity length.

The anisotropic structure of silicon with a 3-fold rotational symmetry around the <111> direction allows a sine-like variation of the vertical sensitivity of $\pm$ 1.5×10^{-11} $(m/s^2)^{-1}$ simply by rotating the spacer azimuthally with respect to the tripod support. The vertical acceleration sensitivity can thus be minimized experimentally. In addition, the base line of the sensitivity can be shifted by the position of the spacer's center ring or by adding some weight on top of the spacer. We see a clear difference between the FEM predictions and the experimental results (triangles in figure 2a) and could not experimentally reach a zero crossing in the vertical vibration sensitivity. Therefore we attached a small silicon ring on top of the spacer (figure 1a) in order to shift the sensitivity curve to a zero crossing. This allows us to optimize the azimuthal angle φ and obtain a residual vertical acceleration sensitivity of $k_z = 0.4(2)\times10^{-12}$ $(m/s^2)^{-1}$. We note the important benefit of being able to minimize the vibration sensitivity via *in situ* adjustment of φ after the manufacturing process has already been completed for the cavity.

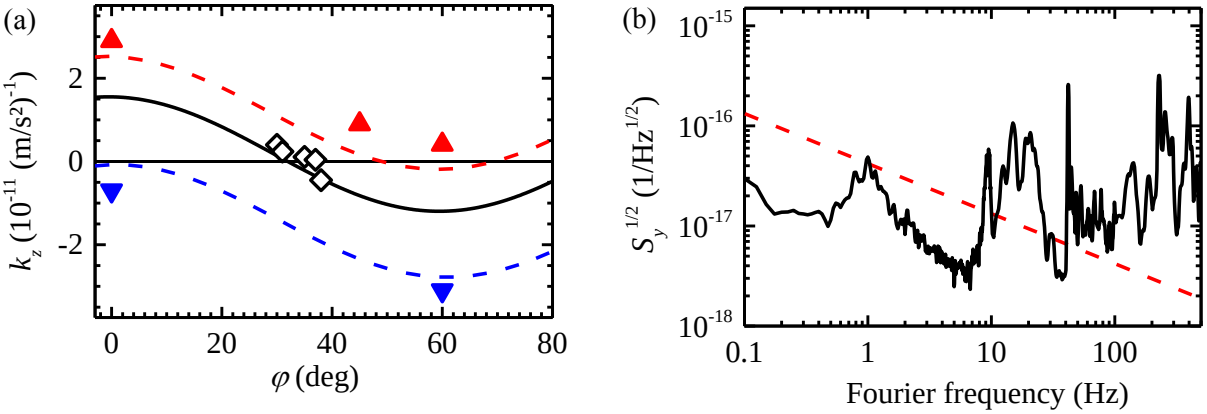

Figure 2. (a) Measured (symbols) and simulated (lines) vertical acceleration sensitivity k_z as a function of the azimuthal rotation angle φ. Upward triangles: the spacer in normal position (support plane Δz = 2.8 mm below the transverse symmetry plane), downward triangles: spacer vertically flipped (Δz = 7.5 mm below); open diamonds: spacer in normal position with an additional silicon ring. The error bars are approximated by the size of the symbols. The lines indicate the values predicted by finite element method (FEM). (b) Calculated frequency noise induced by the seismic perturbations assuming uncorrelated vibrations along x, y, z and expected thermal noise (dashed line); (Colour online).

The seismic spectrum during cryostat operation at 123K was measured close to the cavity along three directions and converted to fractional frequency noise spectral density (figure 2b). The corresponding contribution to the frequency instability of the laser system is thus expected to be well below the thermal noise level for averaging times above 0.1 s, as will be discussed in Section 3.

2.2. Temperature stabilization

The impact of temperature fluctuations on the cavity length depends on the operational offset ΔT from the zero-crossing temperature and the slope of the CTE at this point. To reduce cavity temperature fluctuations, we use a system of two concentric heat shields for the silicon spacer, separated by low-thermal-conductivity materials. The outer shield is actively cooled with cold nitrogen gas evaporated from a Dewar. The passive inner shield acts as an additional low pass filter for reducing residual

temperature fluctuations. For improved thermal control and reliable operation precisely at the zero-crossing CTE, the temperature is monitored at several points across the setup (figure 1b): the temperatures at the top and bottom of the heat shields are measured with Pt100 sensors. The temperature of the spacer relative to the inner heat shield is measured with a pair of miniature copper-constantan thermocouples attached to the spacer and to the inner heat shield. This setup allows us to reliably stabilize the cavity temperature to within less than 50 mK of the zero-CTE temperature.

The thermal model of the system described in [11] was extended by including direct heat transfer from the room temperature environment to the inner shield and to the spacer to account for conduction through the sensor wires, and for thermal radiation entering the optical ports. The corresponding coefficients were determined from observed temperature offsets between outer shield, inner shield and spacer to be 82(3) μW/K and 3.1(1) μW/K, respectively. From the temperature evolution recorded while cooling the system to 123 K, we calculate time constants of 6.4 days for the transfer from the outer to the inner shield, and of 3.4 days for the transfer from the inner shield to the spacer.

Temperature data recorded for 10 days was used to evaluate the thermal stability of the spacer. As the expected short-time temperature fluctuations are well below the instrument resolution of 0.1 mK, we applied the thermal model to calculate the temperature fluctuations at the inner shield and cavity from the measured temperature of the outer shield and of the vacuum chamber (figure 3). Assuming a conservative offset value of ΔT = 50 mK from the CTE zero-crossing temperature, with a resulting CTE: $\alpha \approx 8.5\times10^{-10}$ K^{-1}, we calculate the corresponding length fluctuations of the cavity and find that they do not limit the performance of the system for averaging times up to 1000 s.

2.3. Vacuum pressure stability

Variations in the residual gas pressure inside the cavity induce frequency variations through changes of the refractive index. The refractivity of nitrogen at atmospheric pressure and 30 °C is given by $n - 1 = 2.65\times10^{-4}$ [17]. Assuming a linear dependence of the refractive index with pressure, we can estimate the linear dependence of fractional frequency as 2.65×10^{-7} mbar^{-1}. We have experimentally determined this sensitivity by switching off the ion pump and measuring the induced frequency dependence to be approximately 5×10^{-7} mbar^{-1}. The difference between the measured and estimated values is probably due to a different composition of the residual gas and the separation between vacuum gauge and cavity mode. But the difference is sufficiently small that we can confidently estimate the upper bound of the contribution of intracavity pressure fluctuations to the fractional frequency instability of the cavity.

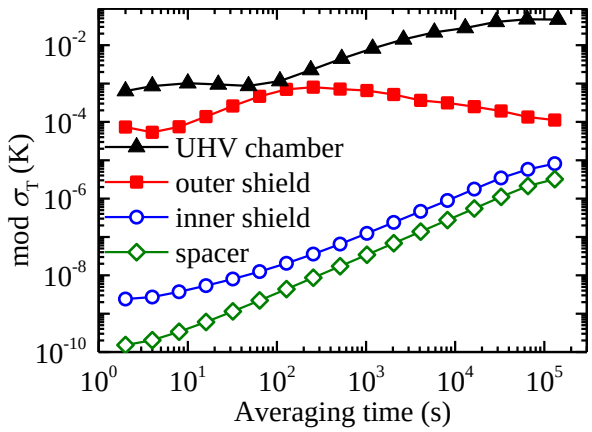

Figure 3. Temperature instability measured on the chamber and the outer shield (filled symbols) and calculated from our thermal model for the inner heat shield and the spacer (open symbols); (Colour online).

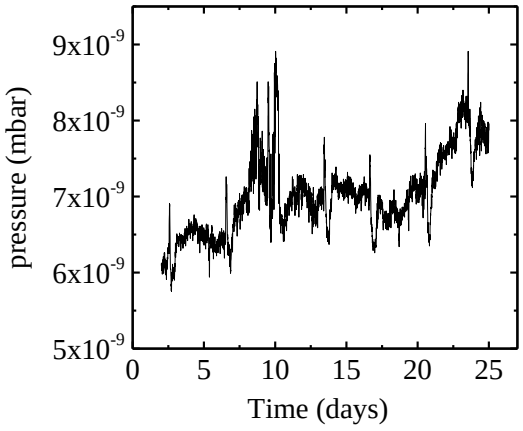

Figure 4. Vacuum pressure recorded for three weeks. The disturbances occurring every 3-4 days are generated by short-time temperature changes of the outer shield during the refilling of the Dewar with liquid nitrogen.

A base pressure in the 10^{-9} mbar range is maintained in the UHV chamber by an ion pump and the cryogenic pumping action of the cold surfaces. An improved vacuum system and ion pump avoid pressure bursts observed in the previous setup [18]. The absolute pressure recorded for three weeks (figure 4) was used to calculate the corresponding instability (figure 5). The increased estimates at lower averaging times could be attributed to noise in the measurement circuit and might be higher than the actual pressure fluctuations. The worsening instability for times above 1000 s could be related to fluctuations arising from daily temperature excursions in the laboratory.

2.4. Residual amplitude modulation

The optical setup is largely identical to the first generation setup described in [8]. A commercial fiber-laser is frequency stabilized to the cavity using the PDH locking technique. The necessary phase modulation is obtained with a Ti-diffused waveguide fiber-coupled electro-optical modulator (EOM) driven with a frequency of 8 MHz. Such EOMs generate relatively large RAM due to imperfect aligning of the polarization maintaining fibers to the principal axes of the birefringent crystal. Thus, the amplitude modulation was controlled by applying a bias voltage to the EOM [19]. The remaining RAM was measured with the PDH lock detector with the laser detuned from the cavity resonance. The observed RAM contribution is clearly below the expected thermal noise limit (figure 5).

3. Frequency stability

All the noise sources presented above contribute to frequency noise at levels well below the expected thermal noise limit for averaging times between 0.1 s to 1000 s, as shown in figure 5. At shorter averaging times, the laser is expected to be limited by vibration-induced noise. At the longer time scales, temperature or pressure instability is expected to limit the laser performance.

In order to measure the laser instability, we have compared the Si stabilized laser with the 698 nm clock laser [7] and with the Sr optical clock transition (figure 5). The frequency of the beat signal was counted with Λ-mode counters [14]. Compared to the modified Allan deviation that we mostly use in this paper the instability of the Sr laser is the regular Allan deviation obtained from a three-cornered-hat measurement. Note that for flicker frequency noise these two deviations are related by mod $\sigma_y \approx 0.82\ \sigma_y$ [20]. For averaging times below 100 s, the instability of the recorded beat signal is very close to be limited by that of the Sr clock laser, while for longer times larger fluctuations are still observed. They are most likely caused by parasitic etalons which will be minimized through optimizing the optical setup.

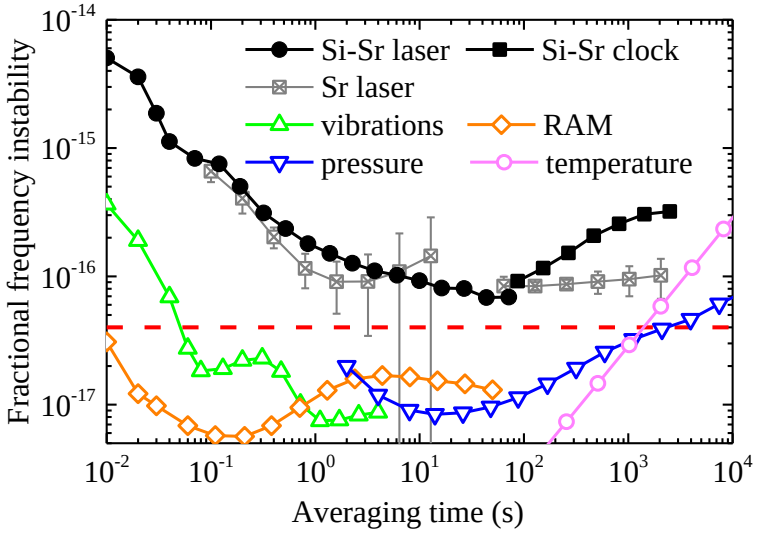

Figure 5. Instability between the silicon system and the Sr laser (full circles) and the Sr clock (full squares), and calculated instabilities due to the discussed noise sources. The instability of the Sr laser from [7] is plotted with crossed squares. Except for the Sr laser instability, which shows overlapping Allan deviation, all other curves show modified Allan deviations. The calculated thermal noise is shown with a dashed line (Colour online).

4. Conclusion and outlook

We have characterized the performance of an updated cryogenic silicon optical resonator by determining the technical noise sources that could potentially contribute to the frequency instability of the laser. The measurements show that the thermal noise floor can be reached for averaging times from tenths of seconds to hours. A frequency comb assisted stability comparison with a state of the art room-temperature ULE resonator stabilized laser at 698 nm was mainly limited by the latter system. We are currently setting up a second cryogenic Si resonator for direct characterization and to push both systems towards their design instability.

Using the same silicon spacer, we can further decrease the thermal noise limit by using low thermal noise crystalline mirror coatings and by decreasing the resonator temperature. Even at 123 K the improved mirror coatings lead to an expected thermal noise limit of mod $\sigma_y \approx 8\times10^{-18}$. Cooling the current cavities to 4 K can reduce the estimated thermal noise to the same value. Combining both approaches has the potential to reduce the thermal noise limit by more than one order of magnitude to the low 10^{-18} level.

Acknowledgments

The cryogenic silicon cavity laser system employed in this work was developed jointly by the JILA Physics Frontier Center (NSF) and the National Institute of Standards and Technology (NIST), the Centre for Quantum Engineering and Space-Time Research (QUEST), and Physikalisch-Technische Bundesanstalt (PTB). We acknowledge funding from the DARPA QuASAR program, the European Community 7th Framework Programme (Grant No. 263500), and the European Metrology Research Programme (EMRP) under QESOCAS. The EMRP is jointly funded by the EMRP participating countries within EURAMET, and the European Union. J. Y. acknowledges support from the Humboldt foundation.

References

[1] Bloom B J, Nicholson T L, Williams J R, Campbell S L, Bishof M, Zhang X, Zhang W, Bromley S L and Ye J 2014 *Nature* **506** 71
[2] Huntemann N, Sanner C, Lipphardt B, Tamm C and Peik E 2016 *Phys. Rev. Lett.* **116**(6) 063001
[3] Dick G J 1988 Local oscillator induced instabilities in trapped ion frequency standards *Proc. 19th Annu. Precise Time and Time Interval Meeting, Redendo Beach, 1987* (Washington, DC: U.S. Naval Observatory) p 133
[4] Thorpe M J, Rippe L, Fortier T M, Kirchner M S and Rosenband T 2011 *Nature Photonics* **5** 688
[5] Norcia M A and Thompson J K 2016 *Phys. Rev. X* **6**(1) 011025
[6] Numata K, Kemery A and Camp J 2004 *Phys. Rev. Lett.* **93** 250602
[7] Häfner S, Falke S, Grebing C, Vogt S, Legero T, Merimaa M, Lisdat C and Sterr U 2015 *Opt. Lett.* **40** 2112–2115
[8] Kessler T, Hagemann C, Grebing C, Legero T, Sterr U, Riehle F, Martin M J, Chen L and Ye J 2012 *Nature Photonics* **6** 687
[9] Wiens E, Chen Q F, Ernsting I, Luckmann H, Rosowski U, Nevsky A and Schiller S 2014 *Opt. Lett.* **39** 3242 and Erratum: 2015 *Opt. Lett.* **40**, 68
[10] Cole G D, Zhang W, Martin M J, Ye J and Aspelmeyer M 2013 *Nature Photonics* **7** 644–650
[11] Hagemann C, Grebing C, Lisdat C, Falke S, Legero T, Sterr U, Riehle F, Martin M J and Ye J 2014 *Opt. Lett.* **39** 5102
[12] Middelmann T, Walkov A, Bartl G and Schödel R 2015 *Phys. Rev. B* **92**(17) 174113
[13] Hagemann C, Grebing C, Kessler T, Falke S, Lemke N, Lisdat C, Schnatz H, Riehle F and Sterr U 2013 *IEEE Trans. Instrum. Meas.* **62** 1556
[14] Benkler E, Lisdat C and Sterr U 2015 *Metrologia* **52** 565

[15] Drever R W P, Hall J L, Kowalski F V, Hough J, Ford G M, Munley A J and Ward H 1983 *Appl. Phys. B* **31** 97–105
[16] Millo J *et al.* 2009 *Phys. Rev. A* **79** 053829
[17] Egan P F, Stone J A, Hendricks J H, Ricker J E, Scace G E and Strouse G F 2015 *Opt. Lett.* **40** 3945
[18] Hagemann C 2013 *Ultra-Stable Laser Based on a Cryogenic Single-Crystal Silicon Cavity* Ph.D. thesis Fakultät für Mathematik und Physik der Gottfried Wilhelm Leibniz Universität Hannover
[19] Zhang W *et al.* 2014 *Opt. Lett.* **39** 1980
[20] Rubiola E 2005 *Rev. Sci. Instrum.* **76** 054703